Hindawi
Journal of Electrical and Computer Engineering
Volume 2022, Article ID 5921691, 13 pages
https://doi.org/10.1155/2022/5921691

Research Article

A Flexible Wearable Thermography System Based on Bioheat Microsensors Network for Early Breast Cancer Detection: IoT Technology

Achraf Elouerghi,[1] **Larbi Bellarbi**,[1] **Zakaryae Khomsi**,[1] **Atman Jbari**,[1] **Abdelhamid Errachid**,[2] **and Nourdin Yaakoubi**[3]

[1]*E2SN, Research Center in Sciences and Technologies of Engineering and Health, National School of Arts and Crafts, Mohammed V University, Rabat, Morocco*
[2]*Institut des Sciences Analytiques (ISA), Claude Bernard University Lyon 1, Villeurbanne, France*
[3]*LAUM Laboratory, Université du Maine, 72085 le Mans cedex 9, Le Mans, France*

Correspondence should be addressed to Achraf Elouerghi; achraf_elouerghi@um5.ac.ma

Received 27 October 2022; Revised 11 December 2022; Accepted 13 December 2022; Published 22 December 2022

Academic Editor: Gurvinder S. Virk

Many women diagnosed by traditional screening methods, such as palpation, mammography, and MRI, do not discover their cancer until it is relatively advanced. This makes treatment more difficult and reduces the chance of a cure. To deal with this issue, we have developed a noninvasive embedded thermography system that allows for an early detection of breast cancer. Indeed, the surface temperature distribution of the breast, which we will call the thermal image, can be used as a preventive indicator of the subsequent development of a cancerous tumor. This is due to the metabolic activity of the immune system, which induces, in the presence of cancer cells, a local increase of temperature even before the tumor tissue is differentiated and detectable by conventional imaging systems. The proposed system is designed as a network of bioheat microsensors applied to the breast, to measure periodically the temperature gradients on the surface. All the bioheat microsensors are addressed by a microcontroller via the I2C protocol. To calibrate and evaluate the proposed system, we have proposed an experimental model of the breast, inside which we have placed Joule effect heating elements.

1. Introduction

Breast cancer is the most common cancer affecting women, with more than 1.7 million new cases diagnosed each year around the world. It is a major public health problem and a dramatic event in a woman's life. In Morocco, its incidence is constantly increasing, and the risk for a woman to develop a breast cancer during her lifetime is about 1 in 10 [1]. This is an alarming figure that increases with age! To reduce the death rate, the interest of early breast cancer detection has been widely demonstrated after several randomized trials. Indeed, the earlier the detection, the greater the chance of cure and, consequently, many lives would be saved: nine out of ten cases, according to general statistics [1].

Among the standard breast cancer detection systems there are:

(i) X-ray mammography: this system is applied to the breast and compresses it between two armatures to obtain mammograms. This technique presents several disadvantages, such as the traumatic and ionizing nature of the X-rays and the high cost of imaging equipment. Moreover, depending on the age of the patient, the density of tissues, and the efficiency of the radiologist, it can sometimes lead to a high rate of false results [2]. Currently, there are ongoing works aimed at optimizing the results of this breast imaging modality based on new optimization algorithms, such as multiobjective and

electromagnetism-like (EML) proposed by researchers Ittannavar and Havaldar [3] and Pezeshki [4] for the segmentation of tumors with high resolution and precision from mammographic images collected by dedicated databases.

(ii) Magnetic resonance imaging (MRI): this system is based on the excitation of hydrogen protons by a strong electromagnetic field. MRI has several limitations such as its specificity is lower than its sensitivity, which means that the number of false positives is relatively high. Another major disadvantage is the very high cost of the examination and follow-up by MRI [5]. However, nowadays, there are improvements have been made on this type of imaging, indeed, research work that has been proposed by Militello et al. [6] and Piantadosi et al. [7] showing that the magnetic resonance imaging modality by intravenous injection of a contrast agent that has paramagnetic properties as gadolinium Gb3+ (DCE-MRI), by the application of deep learning approaches (computer aided detection/diagnosis (CAD)) of algorithms like spatial Fuzzy C-Means (sFCM) and deep convolutional neural network (CNN), namely, U-Net, SegNet, for breast tissue segmentation providing promising results for breast cancer diagnosis.

(iii) Ultrasound: Ultrasound-based systems are also used; however, a tumor could only be detected by these techniques at an advanced stage of differentiation of its tissue from normal tissue [8], which does not have the quality of an early and efficient detection technique.

(iv) PET scan (positron emission tomography imaging) is a medical imaging technique that consists of injecting a radioactive tracer into the body to study the activity of an organ. Although the quantity of radioactivity is minimal and without any noticeable danger for the organism, the process remains rather heavy: nonembedded system, very heavy and expensive diagnostic equipment, very complex logistics of transport, storage, and use of radioactive products, in addition to the relatively long diagnosis time and the need for real time intervention by a specialist [9].

(v) Breast thermography: This is a promising technique that consists of measuring thermal gradients resulting from metabolic activities in the breast. Indeed, the presence of cancer cells induces an increase of temperature compared to normal breast tissue [10, 11]. Comparative studies of screening methods (see Table 1) have shown that the breast thermography is the most effective noninvasive method in terms of sensitivity and specificity, regardless of age, with sensitivity and specificity rates of 95% and early detection up to 10 years in advance [12, 13].

Moreover, in recent years, the biomarkers have been the subject of a large number of developments and have reached a high degree of efficiency [14]. However, despite their interest, they do not allow the localization of the position or extension of a tumor, which is not sufficient for the doctor to act. The nanobiotechnology offers interesting results [15]. Its implementation is currently under test, due to the complexity of the reactions in biological systems, which must first be clarified and understood.

1.1. Aim of the Work. In this article, we propose a noninvasive system, which we have called wearable system of thermography, thanks to which it is possible to measure and map the thermal change observed on the surface of the breast, using a flexible bioheat microsensor network with a very high precision and resolution. An embedded processor will allow data acquisition and transfer to a smartphone to visualize the thermal image and communicate with a web server accessible to the patient and the attending doctor [16]. In order to justify the proposed approach, we performed simulations on models based on the physical characteristics of the breast. On the one hand, to study the thermal gradients generated by possible tumors located in different places of the breast, and on the other hand to confirm the thermal impact on the breast surface.

For the experimental tests, we designed a new prototype of this system and built a breast phantom with a half-spherical structure respecting the physicothermal properties of breasts, on which we apply the wearable system of thermography. In the following, we describe the details of the proposed system, which represents an innovative contribution with low cost, easy to use, and accessibility to all women in order to fight against breast cancer.

2. Study by Numerical Simulation of the Thermal Impact on the Surface Caused by a Thermogenic Tumor

The breast is an organ maintained by the skin. It represents a smooth and supple peripheral zone, and its form varies with age, parity, and ethnicity. As depicted in Figure 1(a), the breast is composed of glandular tissue, fibrous and fatty tissue located between the glandular lobes and lobules, blood and lymph vessels, nerves, and muscles.

A simplified model of the breast, widely used by many authors, considers the breast as a half-spherical structure of a glans placed on a muscle and covered with a layer of fat enveloped by thin layers of skin, as shown in Figure 1(b). With this model and around the OY axis crossing the nipple, we approximate the breast to a multilayered planar structure in order to investigate the heat effect on the surface of a round tumor of several masses placed at different depths. For

Table 1: Comparison between the different screening methods of breast cancer [12].

Methods	Ages	Sensitivity (%)	Large multiple (%)
Mammography	Effective for women older than 50	67.8	88.2
MRI	Effective for women older than 30 years old	86–99	21–97
Ultrasound	Effective for women older than 25 years old	13–98.4	67.8–94
PET	Effective for women older than 25 years old	96	99
Thermography	Effective for all age groups	95	95

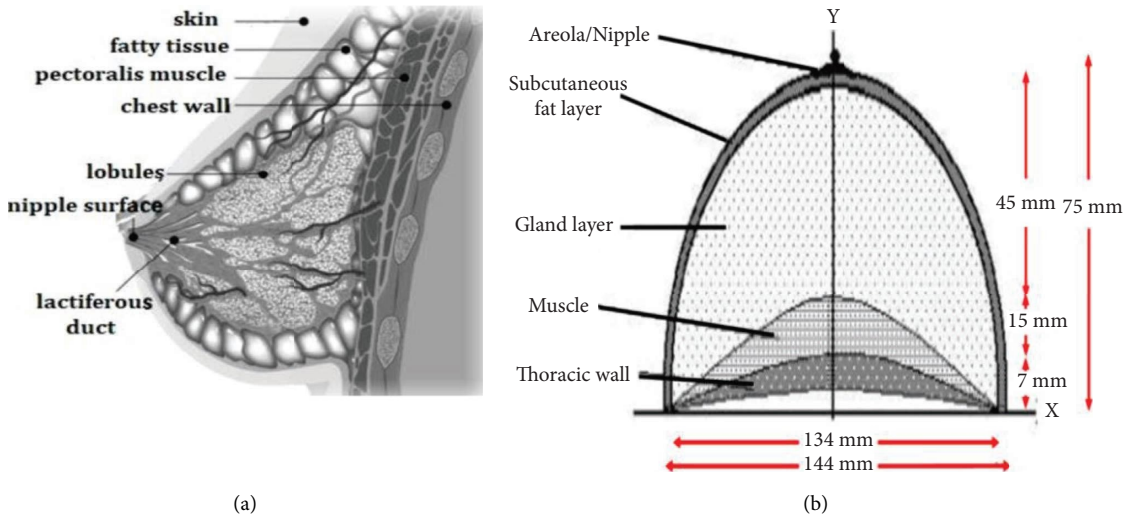

Figure 1: (a) Sagittal section of breast and anterior chest wall and (b) Cross-sectional view of physical domain composition of the breast.

this purpose, an analytical approach consists of using the Pennes bioheat equation [17], which is a mathematical model describing the quantitative relationship between blood flow and tissue temperatures. This equation is given by

$$k.\nabla^2.T - \rho_b.c_b.\omega_b.(T - T_a) + \dot{Q}_m = \rho c \frac{\partial T}{\partial t}, \quad (1)$$

where k is the effective thermal conductivity, ρ_b is the blood mass density, C_b is the specific of blood, ω_b is a term that represents the blood perfusion rate, $\dot{Q}_m$ is the volumetric metabolic heat generation rate, T_a is the arterial temperature, T is the unknown temperature inside the biological tissue. Biological tissue properties density and specific heat are given by ρ and c. The temperature distribution would be simulated by solving (1). The boundary conditions are described as follows:

(i) The continuity of both heat flux and temperature at the interface of tissue layers is described by the following equations:

$$T_n = T_{n+1},$$
$$k_n \frac{\partial T_n}{\partial \eta} = k_{n+1} \frac{\partial T_{n+1}}{\partial \eta}, \quad (2)$$

where η represent the direction perpendicular to the surface.

(ii) Considering the lower part of the muscle layer is assumed to be at a core body temperature such as

$$T = T_c = 37^{\circ}C. \quad (3)$$

(iii) At the skin surface, the thermal boundary condition was expressed as

$$-k \frac{\partial T}{\partial \eta} = h_f (T_s - T_f), \quad (4)$$

where h_f represent the heat convection coefficient between the surrounding air and the skin surface. T_f is the temperature of the surrounding air, T_s is the surface temperature of skin.

Nevertheless, for reasons of efficiency and saving time, we have preferred to use the COMSOL multiphysics software to solve these equations.

The simulations carried out by this software, as depicted in Figure 2, show that a 1 cm diameter tumor located 2.5 cm deep, can create a gradient on the surface that is significantly higher than the sensitivity of the proposed bioheat microsensors and, therefore, can be easily detected [18].

These encouraging results have allowed us to build a first prototype of a wearable system of thermography, as well as a breast phantom, on which measurements will be carried out in order to confirm experimentally the interest of the proposed system.

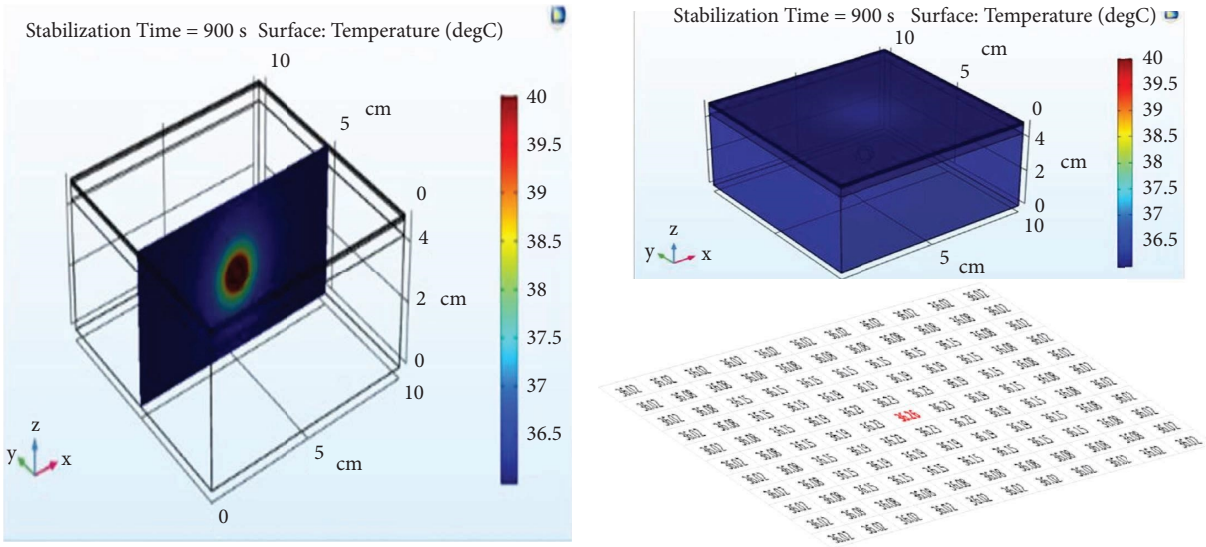

(a) (b)

Figure 2: Thermal distribution from a 25 mm depth tumor (a) Sectional view XZ of 1 cm diameter tumor included at 2.5 cm in depth and (b) Surface temperature distribution with 1 cm tumor located 2.5 cm deep, after a stabilization time of 900 s.

3. Wearable System of Thermography Prototype Descriptions

The embedded breast imaging system, which we call wearable system of thermography is built on a flexible star-shaped surface, using 28 miniature biosensors (Figure 3(b)) positioned to cover the most sensitive areas of the breast, as demonstrated in Figure 3(a).

These bioheat microsensors, compliant with the ASTM E1112 standard, are chosen because of their miniature size as they are designed in thin-layer technology (SMD) for surface assembling, their low supply current avoiding their heating, and their optimization around 37°C, so they can be used in biomedical applications, with the accuracy of 0.1°C. In addition, they offer the possibility of being addressable via the I2C protocol.

To scrutinize the 28 bioheat microsensors, via the I2C protocol, we have developed a program in the Python language, using a microcontroller (MCU) as a processing and transfer unit. Thus, the temperature readings provided by the bioheat microsensors are transformed into the thermal maps using a graphic library called Open Computer Vision (Open CV).

Figure 4 illustrates the design principle of this prototype.

The choice of a flexible support permits to adapt the bioheat microsensor network to the breast shape, thus forming what we called wearable system of thermography.

4. Phantom Design

To validate the concept of the wearable system of thermography for early breast cancer detection, it was necessary to design a mammary phantom imitating the internal structure of the breast according to the physical model given in Figure 1(b) (skin-fat-gland-muscle and thoracic wall). This is achieved by using artificial environments with physical characteristics similar to those of the breast (see Table 2).

However, considering the complexity to realize such a structure with precision and stability over time, we have opted for a simplified realization. This structure is widely used by many authors, which consists of a gelatin half-sphere with a radius of 60.5 mm and enveloped by a silicone layer of 1 mm thickness [18].

Moreover, after comparison by simulation of the thermal gradients induced on the surface by a tumor in the case of these two structures, we did not notice any significant difference compared to the sensitivity of the sensors.

Figure 5 shows the distribution of surface temperature gradients for two models of the breast phantom when incorporating a nipple tumor located at a depth of 15 mm.

A second simulation represents the surface thermal gradient distribution for both breast phantom models with a tumor located at 20 mm depth on the LOQ quadrant, as shown in Figure 6.

A third simulation was performed to target the UIQ quadrant with a fixed tumor depth of 30 mm. Figure 7 illustrates the surface thermal gradient distribution for both models.

In conclusion, after these comparisons carried out between the approximated and simplified phantom model, we can be satisfied for the rest of the work with a simple model to design and build a breast phantom, in order to experiment the proposed wearable system of thermography.

5. Experimental Setup

To create the thermal gradients inside this breast phantom and simulate the presence of tumors, we have immersed heat sources by Joule effect in the gelatin (gland). They are shaped

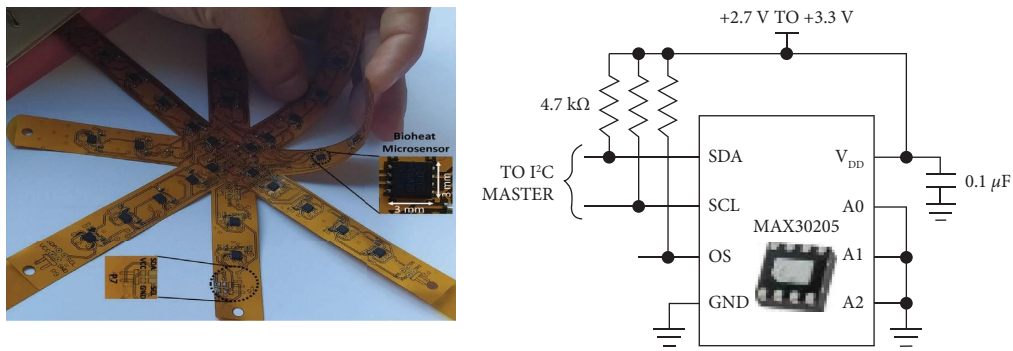

Figure 3: Photographs of bioheat microsensors network (a) Flexible card with a bioheat microsensors network and (b) Used bioheat microsensors.

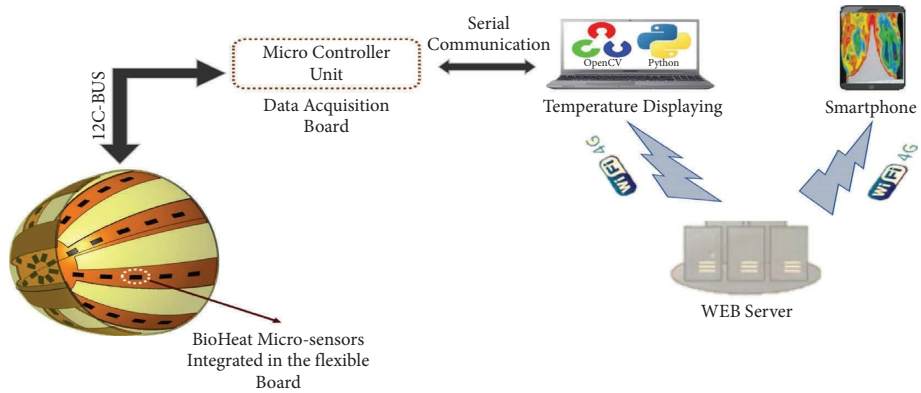

Figure 4: Block diagram of the configuration of the noninvasive measurement system.

Table 2: Physical and geometric characteristics of the simplified breast model [19].

	Silicone (skin)	Gelatine (gland)	Thermal resistance (tumor)
h (mm)	1.6	60.9	—
k (W/mK)	0.22	0.43	0.52
ρ (kg/m^3)	1200	1050	1430
c (J/kgK)	3589	3070	1150

as miniature resistors electrically isolated and fixed at different heights on a FR4 board on which the phantom is placed.

To control the temperature around these resistors assimilated to artificial tumors, we used a reference resistor of the same type, on which we stuck the bioheat microsensors of the same type as those used on the surface. Thus, we can consider that any resistor supplied with the same current as the reference resistor, will create the same temperature in its proximity. Therefore, we can simultaneously control the temperature of each artificial tumor by controlling of the supply current. Figures 8(a) and 8(b) shows the support made of FR4, with the reference resistor and the three heating resistors of 100 Ω of the SMD type. These resistors are distributed in different zones of the phantom, such as nipple, lower outer quadrant (LOQ), and upper inner quadrant (UIQ), with the depths of 15 mm, 20 mm, and 30 mm (Figure 8(a)). The artificial gland is molded on the made support to constitute the final phantom, as depicted in Figure 8(b).

Figure 9 shows the experimental bench used to evaluate the principle of wearable system of thermography applied to the right breast. The temperature of the 4 sources is controlled by a current control system with potentiometers.

5.1. Thermal Stability of the Test Bench. To ensure the thermal and physicochemical stability of the phantom, without it being thermally isolated from the surface thermal sensors, we covered it with a very thin layer of flexible plastic. In addition, before performing an experimental test, we ensure, first of all, that the temperature of the phantom has stabilized with respect to the ambient temperature T_a of the room, which is equal to 23.97°C, as shown in Figure 10.

Similarly, we ensure that the temperature around the reference tumor is stable, after having fixed the supply current of the corresponding reference resistor.

Figure 11 illustrates that the temperature measured using the biomicro sensor stabilizes at the desired temperature, i.e.

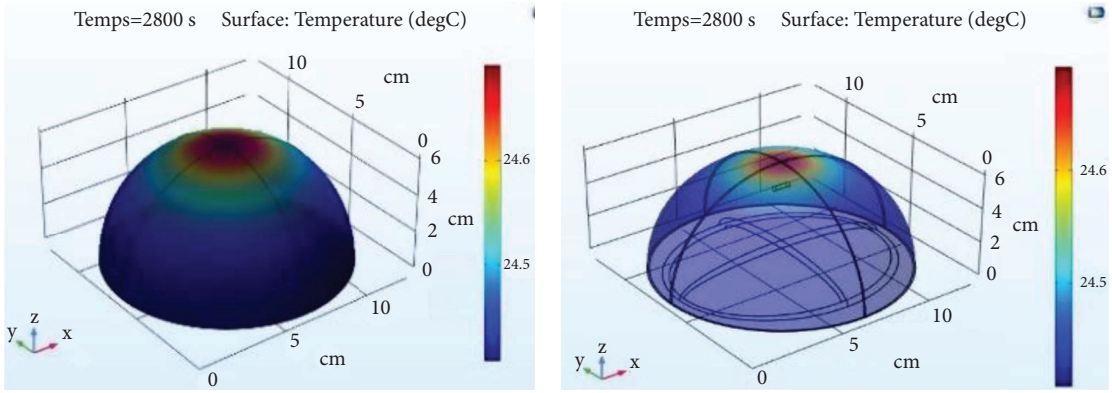

(a) (b)

Figure 5: Thermal distribution from a 15 mm depth tumor (a) Simplified phantom model and (b) Approximated phantom model.

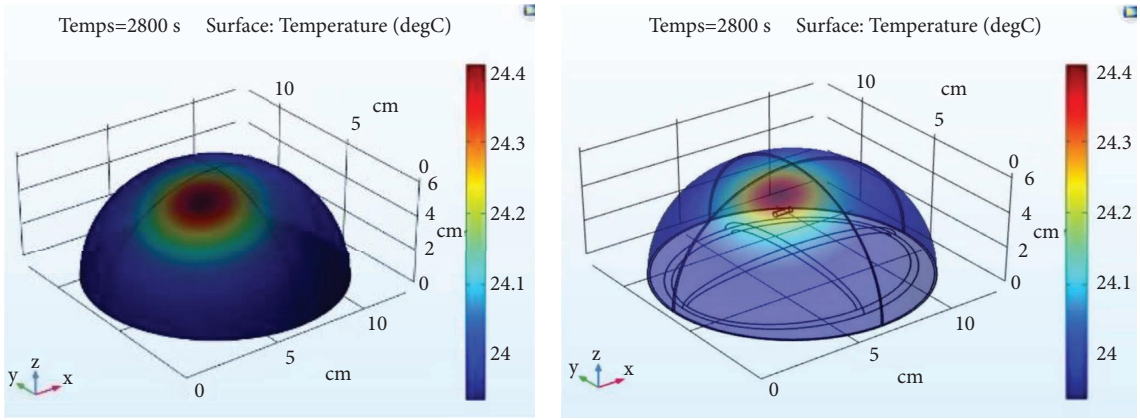

(a) (b)

Figure 6: Image of breast phantom with LOQ tumor (a) Simplified phantom model and (b) Approximated phantom model.

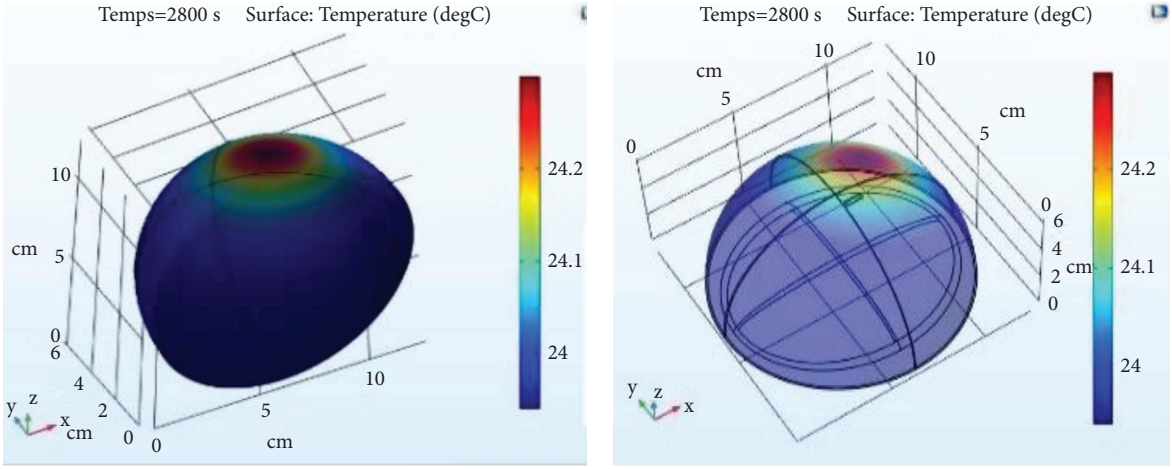

(a) (b)

Figure 7: Image of breast phantom with UIQ tumor (a) Simplified phantom model and (b) Approximated phantom model.

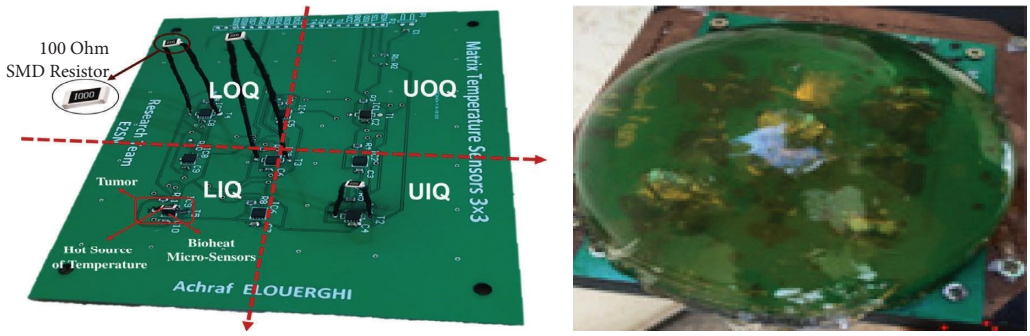

Figure 8: Support realized (a) FR4 PCB board with hot source of temperature and bioheat microsensors and (b) Combination of board and phantom.

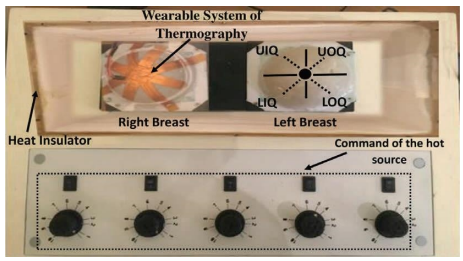

Figure 9: Experimental bench for the evaluation of THBC.

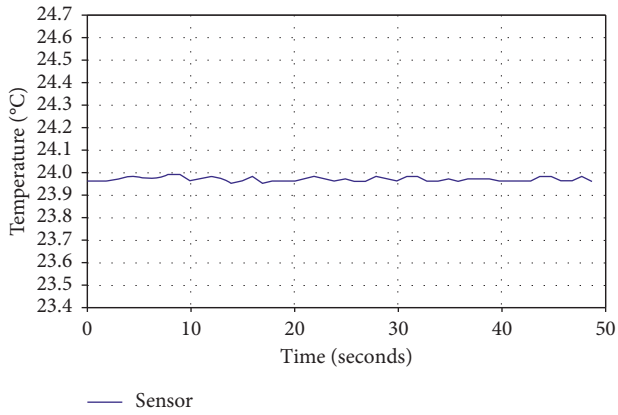

Figure 10: Thermal stability of the phantom.

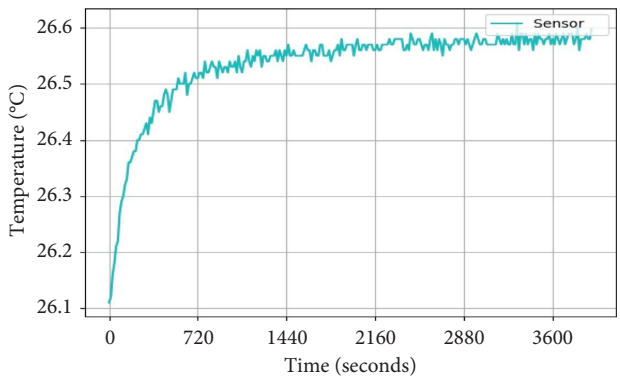

Figure 11: Temperature stabilization curve of the reference tumor.

26.6°C, after an hour of fixing the current value, with a fluctuation lower than 0.1°C.

It should be noted that this technique allows us to ensure that the supply current to each resistor is the image of the temperature of each tumor, respectively.

6. Results of Experimental Testing of the Prototype

Figure 12 shows how we adapted the prototype of the wearable system of thermography to the breast phantom. The 28 miniature bioheat sensors are positioned to cover the most vulnerable zones of the breast. Similarly, we assigned a reference to each bioheat microsensor in order to identify it on the wearable system of thermography, as well as its corresponding point on the surface of the right breast phantom.

Let us specify that the choice of the distance of 1.5 cm between bioheat microsensors was based on a research using COMSOL multiphysics software. Indeed, according to the simulations carried out, the minimum distance between 2 points so that their thermal gradient is greater than the maximum sensitivity of the bioheat microsensor is 1.5 cm, i.e., 0.1°C (bioheat microsensor precision).

Figure 12 illustrates the bioheat microsensors placed on the surface of the phantom. These bioheat microsensors are connected to the I2C BUS (SDA and SCL) to acquire data in real time. The data will be processed afterwards using Python language through the MCU processing unit.

To experimentally evaluate the proposed wearable system of thermography to detect breast cancer at an early stage, we considered the left breast as reference by maintaining it at the ambient temperature, and the right breast as a target by feeding one of the heating resistors to increase its temperature in order to simulate a tumor.

Figure 13 shows the temperature distribution on the surface of the left breast phantom (reference) measured by randomly chosen bioheat microsensors and which remains equal to 24°C, with a fluctuation of $\Delta T << 0.1$°C.

It should be noted that we have considered the ambient temperature as a reference temperature to minimize the heat exchange with the outside.

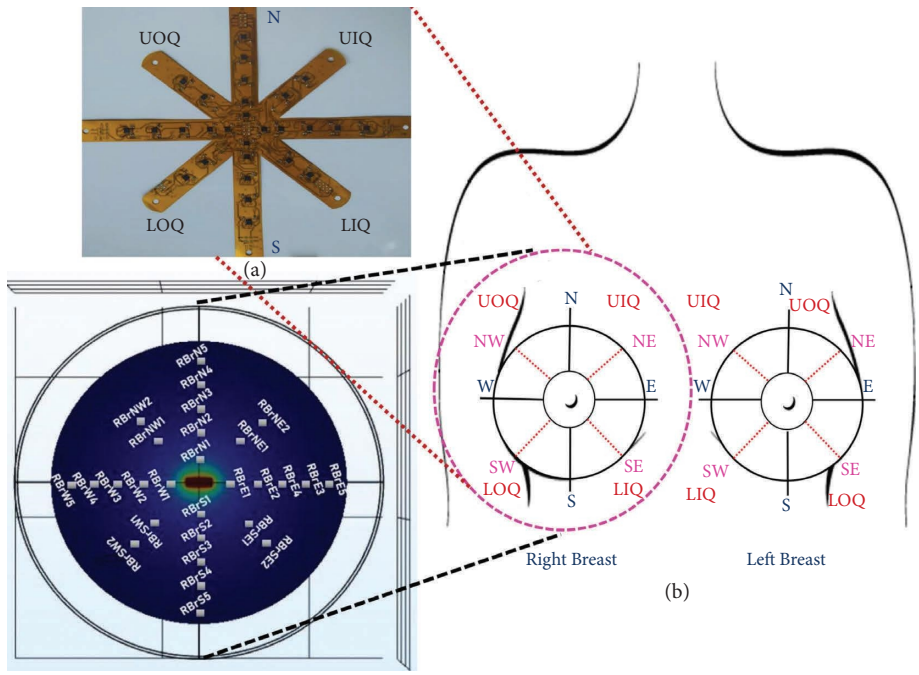

Figure 12: Photographs of bioheat microsensors network (a) Flexible card with a bioheat microsensors network and (b) Position of bioheat microsensors network on breast.

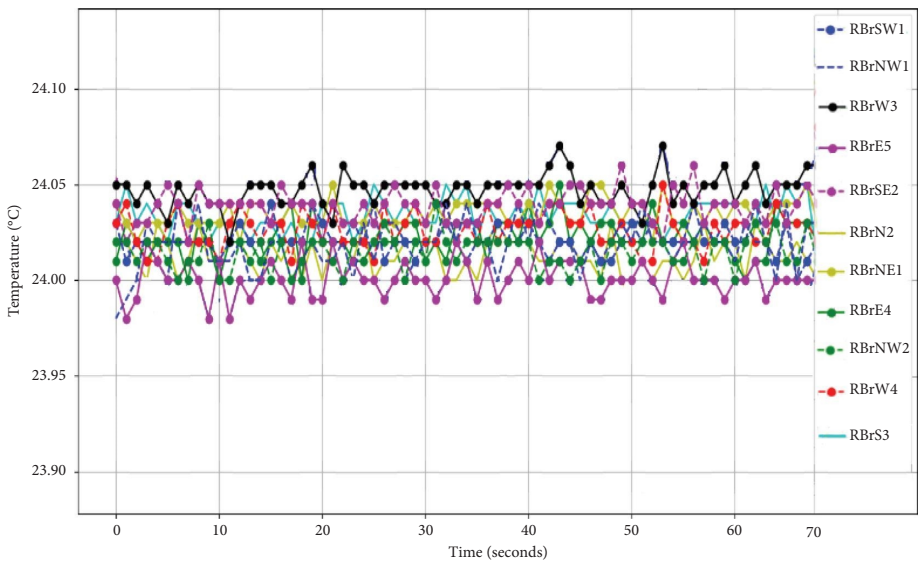

Figure 13: Temperature variation in several bioheat microsensors for the normal phantom.

Figure 14 shows, after stabilization of the gradients, the temperatures obtained by the 28 bioheat microsensors distributed on the surface of the right breast using an artificial tumor located at the nipple with a depth of 15 mm and a temperature of 26.7°C.

The temperature decreases toward the ambient temperature as the distance from the nipple increases. This is the case for the RBrW5, RBrSW2, RBrNW2, and RBrN5 bioheat microsensors covering the extremities of the phantom. Thus, we note a maximum difference detected at the breast phantom surface of $\Delta T_{max} = +0.6$°C.

In order to simplify the reading of the thermal gradients of the breast, we have developed a graphical interface using the OpenCV library, which allows to illustrate the gradients as a radial distribution of colors from blue (cold zones) to red (hot zones). Figure 14(b) shows a graphical representation of the measurements depicted in Figure 14(a), which can be also displayed on the patient's smartphone, which

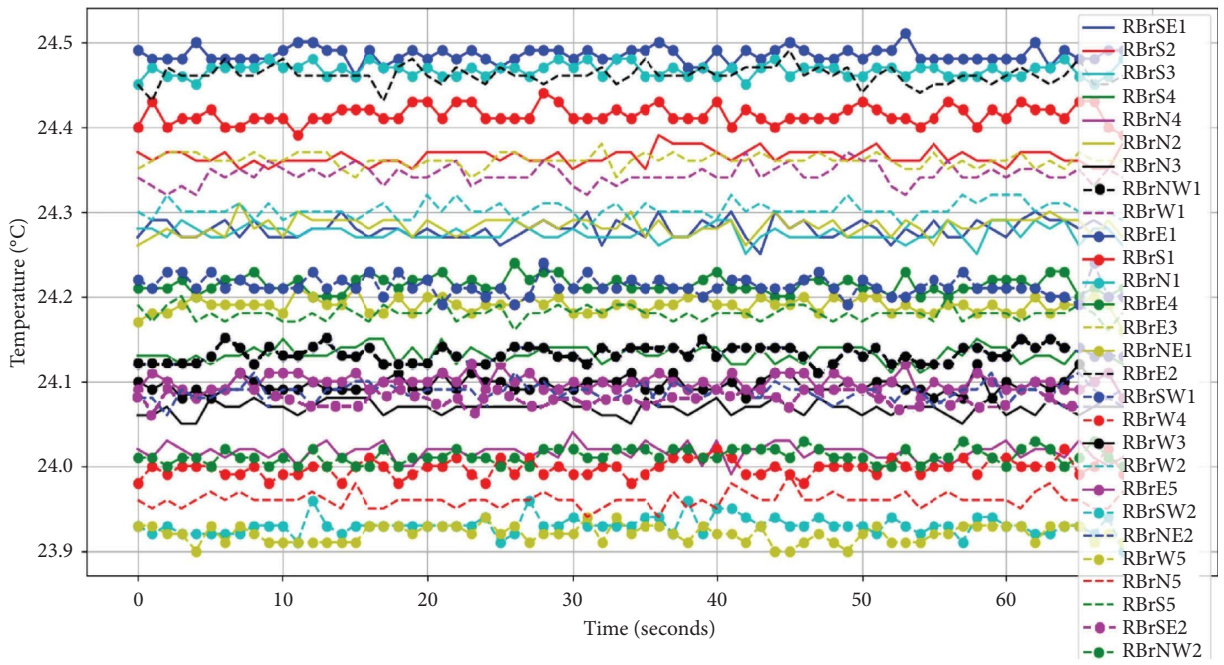

(a)

(b)

Figure 14: Temperature distribution of the right breast phantom with a nipple tumor integrated at 15 mm. (a) Variation in several bioheat microsensors and (b) thermal distribution with OpenCV on smartphone board.

provides a user-friendly visual illustration, as well as a connection interface with a server for recording and processing the data of each patient.

Figure 15 illustrates the measurements obtained by the 28 bioheat microsensors distributed on the surface of the cancerous right breast when heating the resistor located at the area covered by the RBrSW2 and RBrSW1 bioheat microsensors with a depth of 20 mm and a temperature of 26.7°C. The maximum temperature measured by the RBrSW2 and RBrSW1 bioheat microsensors located directly over the tumor is 24.5°C.

Moving towards the extremities of this quadrant (LOQ), for the RBrS4, RBrN1, RBrE1, and RBrE2 bioheat microsensors, the temperature stabilizes at ambient temperature, i.e. 24°C. Thus, we note a maximum difference detected at the breast phantom surface of $\Delta T_{max} = +0.5$°C.

Figure 15(b) presents a graphical representation of the measurements obtained in Figure 15(a), which clearly displays the hot zone.

Considering the opposite side, Figure 16(a) depicts the measurements collected by the 28 bioheat microsensors distributed on the surface of the right cancerous breast, when heating to 26.7°C the resistance located at the UIQ zone is covered by the RBrNE1, RBrNE2, and RBrE2 bioheat microsensors located at a depth of 30 mm. The maximum temperature measured by the bioheat microsensors

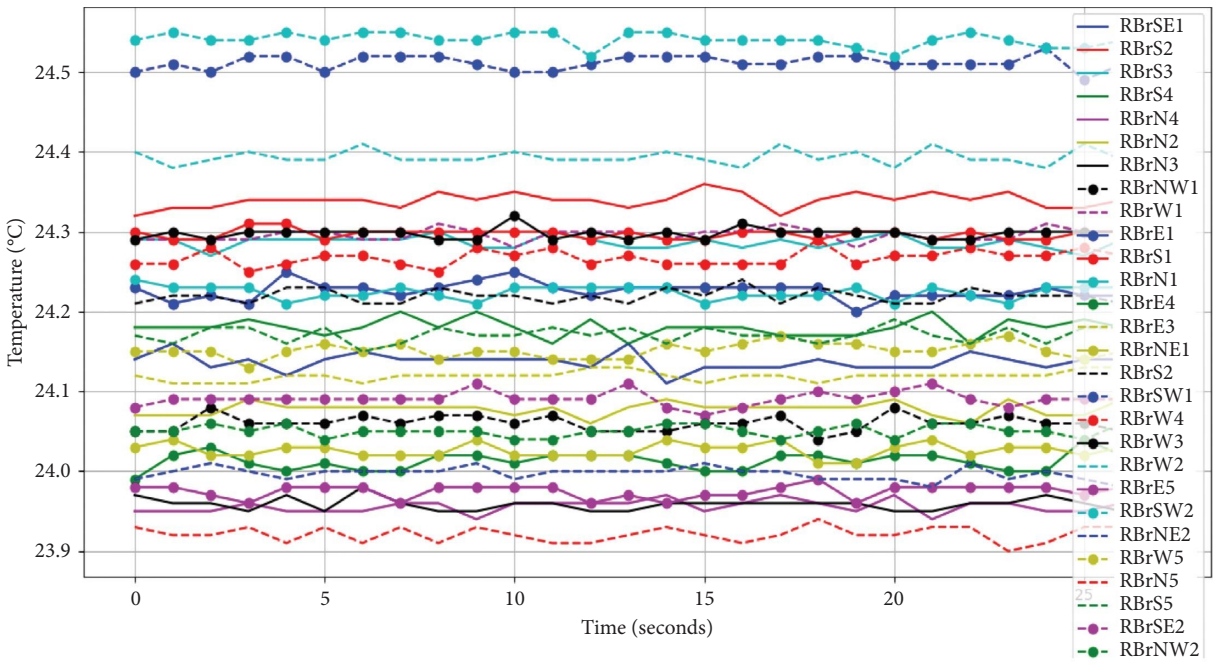

(a)

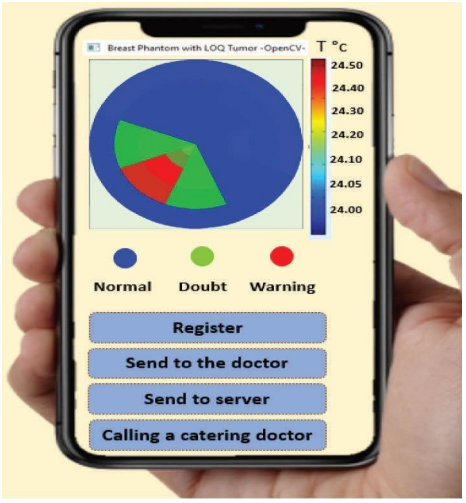

(b)

Figure 15: Temperature distribution of the right breast phantom with a lower outer quadrant (LOQ) tumor integrated at 20 mm (a) Variation in several bioheat microsensors and (b) thermal distribution with OpenCV on smartphone board.

(RBrNE1, RBrNE2, and RBrE2) located directly over the artificial tumor is 24.32°C. Moving towards the extremities of this quadrant (UIQ), for both the RBrE5 and RBrN5 bioheat microsensors, the temperature stabilizes at 24.10°C, i.e. +0.1°C compared to the temperature of the left breast which is always maintained at 24°C. Hence, we note a maximum gradient detected at the surface of the breast phantom up to $\Delta T_{max} = +0.45$°C.

Figure 16(b) displays a graphical representation of the measurements shown in Figure 16(a), which shows very clearly the displacement of the hot zone towards the opposite side.

In Table 3, we present comparison results of temperature gradients on the surface of the breast phantom, obtained by simulation and by experimental measurements, for the different positions of a tumor (nipple, UIQ, and LOQ).

By observing the measurements given in Table 3, we can verify that the tumors are easily detectable, whatever the area and depth (Nipple, LOQ, or UIQ) with a precision of 0.1°C.

Moreover, it is interesting to mention here the advantage of the proposed approach compared to infrared camera thermography, which is used to measure variations in breast surface temperature with a precision of 0.1°C [20, 21] for early breast cancer detection. Indeed, with this latter, the

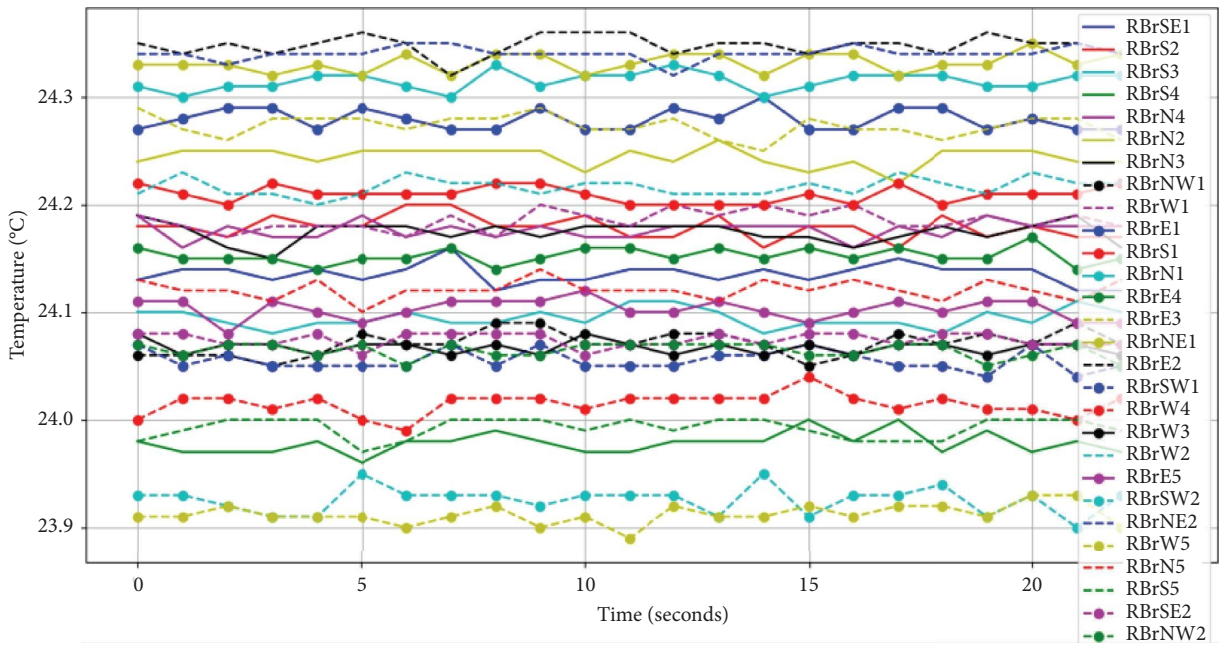

(a)

(b)

Figure 16: Temperature distribution of the right breast phantom with an upper inner quadrant (UIQ) tumor integrated at 30 mm (a) Variation in several bioheat microsensors and (b) thermal distribution with OpenCV on smartphone board.

Table 3: Comparative results of the abnormal breast phantom.

Tumor location	Nipple	LOQ	UIQ
Bioheat microsensors nearest to tumor	RBrW1, RBrE1, RBrS1, and RBrN1	RBrSW1 and RBrSW2	RBrNE1 and RBrNE2
Thermal gradient measured by COMSOL multiphysics (°C)	24.44	24.40	24.28
Thermal gradient measured by the thermal system test bench (°C)	24.45	24.51	24.32
Errors (°C)	0.01	0.11	0.04

patient must scrupulously respect the measurements conditions, such as remaining isolated and shirtless in a dark and cold room to prevent any air flow towards the patient or thermal noise emitted by the various instruments. Although a stabilization waiting time of about 20 minutes is required before measurements are taken into place [22, 23].

7. Conclusions and Prospects for Future Research

Through this work, we have demonstrated the medical feasibility of a wearable system of thermography for the early breast cancer detection by deploying a hand-held, precise, and noninvasive thermographic system. The effectiveness of this system has been proven, first by several simulations using the COMSOL multiphysics software, which demonstrated the existence of thermal gradients on the surface created by tumors placed in different quadrants and at different depths. Then, the experimental tests carried out on breast phantom.

As perspectives, our future work aims to evaluate and validate clinically this wearable system of thermography by working on target and witness populations proposed by our oncologist partners in Rabat and Casablanca. Furthermore, other configurations of bioheat microsensors are under investigation, as well as the development of an artificial intelligence to explore in real time the gradients measured and to extract a useful diagnosis for the attending doctor and the patient, Indeed, our thermal system allows to map breast images based on a network of microsensors representing the pixels of the thermal image and using a radiomics-guided by deep learning algorithms approach which is integrated into electronic chip of the thermal system to predict the malignancy degree of early stage of breast cancer. Furthermore, researchers such as Militello et al. [24] and Chen et al. [25] have shown the feasibility and importance of computerized systems and the implementation of deep learning models in clinical practice for the characterization and preprocessing of images related to breast lesions.

Data Availability

No data were used to support this study.

Conflicts of Interest

The authors declare that they have no conflicts of interest.

Acknowledgments

This research project was selected for funding under the AL-KHAWARIZMI program, through a call for applied research projects in the field of Artificial Intelligence (AI) and its applications under the subsidy of the Ministry of Industry, Trade and Green and Digital Economy (MITGDE) in partnership with the Digital Development Agency (DDA) and the National Center for Scientific and Technical Research (CNRST).

References

[1] F. Bray, J. Ferlay, I. Soerjomataram, R. L. Siegel, L. A. Torre, and A. Jemal, "Global cancer statistics 2018: GLOBOCAN estimates of incidence and mortality worldwide for 36 cancers in 185 countries," *CA: a cancer journal for clinicians*, vol. 68, no. 6, pp. 394–424, 2018.

[2] R. W. Pinsky and M. A. Helvie, "Mammographic breast density: effect on imaging and breast cancer risk," *Journal of the National Comprehensive Cancer Network*, vol. 8, no. 10, pp. 1157–1165, 2010.

[3] S. S. Ittannavar and R. H. Havaldar, "Segmentation of breast masses in mammogram image using multilevel multiobjective electromagnetism-like optimization algorithm," *BioMed Research International*, vol. 2022, Article ID 8576768, 14 pages, 2022.

[4] H. Pezeshki, "Breast tumor segmentation in digital mammograms using spiculated regions," *Biomedical Signal Processing and Control*, vol. 76, Article ID 103652, 2022.

[5] C. K. Kuhl, S. S. Schrading, C. C. Leutner et al., "Mammography, breast ultrasound, and magnetic resonance imaging for surveillance of women at high familial risk for breast cancer," *Journal of Clinical Oncology*, vol. 23, no. 33, pp. 8469–8476, 2005.

[6] C. Militello, L. Rundo, M. Dimarco et al., "Semi-automated and interactive segmentation of contrast-enhancing masses on breast DCE-MRI using spatial fuzzy clustering," *Biomedical Signal Processing and Control*, vol. 71, Article ID 103113, 2022.

[7] G. Piantadosi, M. Sansone, R. Fusco, and C. Sansone, "Multi-planar 3D breast segmentation in MRI via deep convolutional neural networks," *Artificial Intelligence in Medicine*, vol. 103, Article ID 101781, 2020.

[8] W. A. Berg, J. D. Blume, J. B. Cormack et al., "Combined screening with ultrasound and mammography vs mammography alone in women at elevated risk of breast cancer," *JAMA*, vol. 299, no. 18, pp. 2151–2163, 2008.

[9] T. A. Heusner, S. Kuemmel, L. Umutlu et al., "Breast cancer staging in a single session: whole-body PET/CT mammography," *Journal of Nuclear Medicine*, vol. 49, no. 8, pp. 1215–1222, 2008.

[10] E. C. Fear, S. C. Hagness, P. M. Meaney, M. Okoniewski, and M. Stuchly, "Enhancing breast Tumor detection with near field imaging," *IEEE Microwave Magazine*, vol. 3, no. 1, pp. 48–56, 2002.

[11] V. Zhurbenko, "Challenges in the design of microwave imaging systems for breast cancer detection," *Advances in Electrical and Computer Engineering*, vol. 11, no. 1, pp. 91–96, 2011.

[12] A. Hossam, H. M. Harb, and H. H. Abd El Kader, "Performance analysis of breast cancer imaging techniques," *International Journal of Computer Science and Information Security*, vol. 15, no. 5, pp. 48–56, 2017.

[13] D. A. Kennedy, T. Lee, and D. Seely, "A comparative review of thermography as a breast cancer screening technique," *Integrative Cancer Therapies*, vol. 8, no. 1, pp. 09–16, 2009.

[14] E. C. Porto-Mascarenhas, D. X. Assad, H. Chardin et al., "Salivary biomarkers in the diagnosis of breast cancer: a review," *Critical Reviews In Oncology-Hematology*, vol. 110, pp. 62–73, 2017.

[15] T. C. Jackson, B. O. Patani, and D. E. Ekpa, "Nanotechnology in diagnosis: a review," *Advances in Nanoparticles*, vol. 06, no. 03, pp. 93–102, 2017.

[16] A. Elouerghi, L. Bellarbi, A. Afyf, and T. Talbi, "A novel approach for early breast cancer detection based on embedded micro-BioHeat ultrasensitive sensors: IoT technology," in *Proceedings of the IEEE. International Conference on Electrical and Information Technologies (ICEIT)*, pp. 1–4, Rabat, Morocco, March 2020.

[17] H. H. Pennes, "Analysis of tissue and arterial blood temperatures in the resting human forearm," *Journal of Applied Physiology*, vol. 85, no. 1, pp. 05–34, 1998.

[18] Z. Khomsi, A. Elouerghi, A. Afyf, and A. Bellarbi, "Contribution for the early detection of breast cancer by a superficial thermography solution," in *Proceedings of the IEEE. International Conference on Electrical and Information Technologies (ICEIT)*, pp. 1–4, Rabat, Morocco, March 2020.

[19] A. Chanmugam, R. Hatwar, and C. Herman, "Thermal analysis of cancerous breast model," *ASME International Mechanical Engineering Congress and Exposition*, American Society of Mechanical Engineers, , vol. 2012, pp. 135–143, 2012.

[20] S. V. Francis and M. Sasikala, "Automatic detection of abnormal breast thermograms using asymmetry analysis of texture features," *Journal of Medical Engineering & Technology*, vol. 37, no. 1, pp. 17–21, 2013.

[21] M. Bahador, M. M. Keshtkar, and A. Zariee, "Numerical and experimental investigation on the breast cancer tumour parameters by inverse heat transfer method using genetic algorithm and image processing," *Sādhanā*, vol. 43, no. 9, pp. 142–210, 2018.

[22] A. Morales-Cervantes, E. S. Kolosovas-Machuca, E. Guevara et al., "An automated method for the evaluation of breast cancer using infrared thermography," *EXCLI journal*, vol. 17, pp. 989–998, 2018.

[23] S. Pramanik, D. Banik, D. Bhattacharjee, M. Nasipuri, M. K. Bhowmik, and G. Majumdar, "Suspicious-region segmentation from breast thermogram using DLPE-based level set method," *IEEE Transactions on Medical Imaging*, vol. 38, no. 2, pp. 572–584, 2019.

[24] C. Militello, L. Rundo, M. Dimarco et al., "3D DCE-MRI radiomic analysis for malignant lesion prediction in breast cancer patients," *Academic Radiology*, vol. 29, no. 6, pp. 830–840, 2022 Jun.

[25] W. Chen, M. L. Giger, G. M. Newstead et al., "Computerized assessment of breast lesion malignancy using DCE-MRI," *Academic Radiology*, vol. 17, no. 7, pp. 822–829, 2010 Jul.

[26] S. V. Francis, M. Sasikala, and S. D. Jaipurkar, *Detection of Breast Abnormality Using Rotational Thermography", Application of Infrared to Biomedical Sciences*, pp. 133–158, Springer, Singapore, 2017.

[27] Y. He, B. Deng, H. Wang et al., "Infrared machine vision and infrared thermography with deep learning: a review," *Infrared Physics & Technology*, vol. 116, Article ID 103754, 2021.